JOURNAL OF APPLIED ELECTROCHEMISTRY 26 (1996) 431–437

A novel procedure in the galvanic deposition of Zn alloys for the preparation of large area Ni and Ni–Co surfaces

S. A. S. MACHADO, J. TIENGO, P. DE LIMA NETO, L. A. AVACA

Departamento de Físico-Química, Instituto de Química de São Carlos - USP, C.P. 780, 13560-970 São Carlos-SP, Brazil

Received 29 May 1995; revised 13 September 1995

A new methodology for the electrodeposition of Ni–Zn and Ni–Co–Zn alloys that prevents zinc being in contact with the substrate and allows total elimination of this metal during alkaline leaching is fully described. This is achieved by a careful control of the plating bath composition during the electrolysis. The resulting coatings show a multilayer structure and the desirable concentration profile for all the metallic species involved, as revealed by SEM and EDX analyses. The electrochemical active area of the deposits after leaching of the zinc was measured by cyclic voltammetry. They were of the order of 1100 and 4400 times the geometric area for Ni and Ni–Co, respectively. These highly porous structures are very active for hydrogen evolution in alkaline solutions, showing extremely low overpotentials for relatively high current densities, as well as good stability for long term operation. Other possible applications for these structures are briefly discussed.

1. Introduction

The growing utilization of electrolytic hydrogen in different industries for the production of food, chemicals, fertilizers and also as a nonpolluting fuel option drives electrolysis research towards alternative materials and methods for the production of hydrogen at a lower cost. The development of active electrodes for hydrogen and oxygen production by alkaline water electrolysis may bring a significant improvement in the field.

Active cathodes are usually obtained by either the preparation of metallic surfaces having a large electrochemical active area [1–4] or from alloys showing a catalytic effect for the hydrogen evolution reaction (HER) [1, 5–8]. Some large area nickel alloys are particularly convenient for this purpose due to their high activity and simplicity of preparation [2, 3, 9]. They are produced by either plasma spraying, thermal interdiffusion or electrochemical deposition of nickel together with an amphoteric metal (aluminium, zinc or tin) which is subsequently leached out by alkaline dissolution, leaving a very porous structure [3].

The choice of Zn as one of the components in the alloy has some advantages in relation to Al and/or Sn. First, Zn can be electrochemically codeposited with Ni thus making the cost of production of these cathodes lower than those prepared with Al by plasma spraying or interdiffusion. Secondly, Zn does not form intermetallic compounds with Ni (as in the case of Sn [10]) and is therefore more easily removed from the catalyst surface.

One significant problem that arises when using this kind of porous Ni or Ni alloy cathode is the effect of residual Zn on the activity of the material for the HER. Chen and Lasia [11] observed an enhancement in the activity of Ni–Zn electrodes when the amount of Zn in the deposit was increased by shifting the deposition potential cathodically. The authors attributed this effect to an increase in the electrochemical active area after the leaching of Zn from the material, but no attempt was made to determine the amount of Zn in the final structure. Balej *et al.* [12] prepared several Ni–Zn alloys and measured the hydrogen and oxygen overpotentials (η). They found that the composite with 32–34% residual Zn showed the lowest overpotentials for both reactions. Meanwhile, the absolute values reported for η were much larger than those usually reported.

Among the several possibilities for Ni alloys, this laboratory has been carrying out studies involving Ni–Co–Zn cathodes [3, 6, 9], because of the excellent chemical stability and very high activity towards the HER. However, one of the problems identified in these studies was that with the conventional methodology of electrodeposition, i.e., using a modified Watts bath containing $\sim 30\,g\,dm^{-3}$ $ZnSO_4$, the deposition of a large amount of Zn directly on to the substrate usually resulted in poorly adherent and fragile coatings. This is an almost unavoidable effect due to the anomalous character of Ni/Zn codeposition that promotes the preferential plating of the less noble metal, even when it is present at low concentrations [13].

Moreover, the presence of residual Zn in the final material hinders its application for other purposes, such as controlled oxidation to promote the superficial growth of mixed oxides of the type $NiCo_2O_4$, that are well recognized catalysts for the oxygen evolution reaction [14–16].

With the aim of obtaining highly porous and stable Ni and Ni–Co surfaces free from residual Zn, this

0021-891X

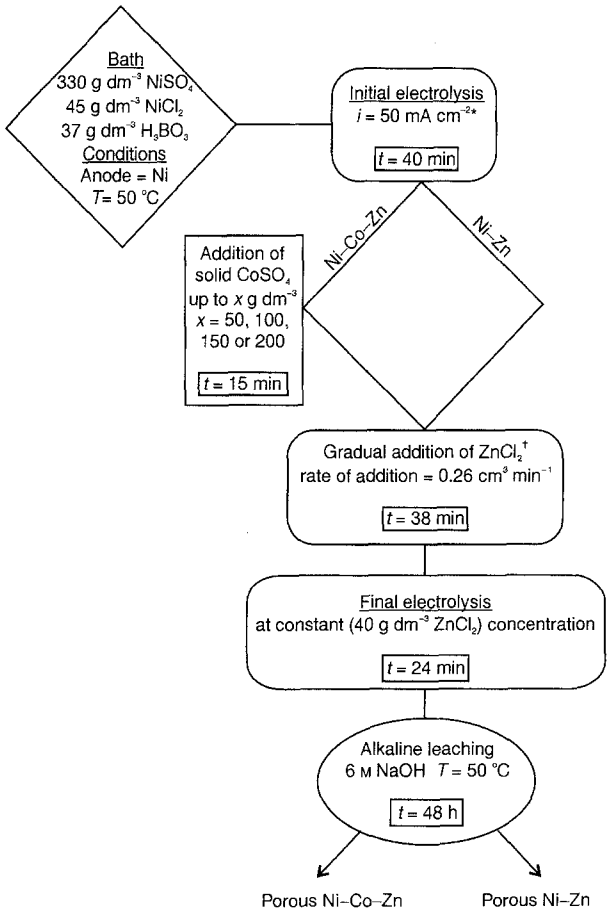

Fig. 1. Flowchart of the deposition methodology.

work describes a new electrodeposition methodology that allows the preparation of surfaces acting either as active cathodes for the HER or as an eventual precursor of mixed oxide anodes for the oxygen evolution reaction.

2. Experimental details

Working electrodes were constructed using mild steel plates (0.102% C, 0.05% Si, 0.62% Mn, 0.09% P, 0.019% S and 0.016% Mg) in the form of discs with 0.3 cm^2 geometric area, embedded in epoxy resin. Prior to the alloy plating, these electrodes were polished with grid 600 emery paper and degreased with KOH. The same treatment was applied to the bright Ni and metallurgical Ni–Co alloy electrodes. The anode was a Ni foil with $\sim 10\,cm^2$ geometric area. For the voltammetric experiments a Pt foil secondary electrode and a Hg/HgO reference system were also used in a conventional three-electrode cell with an appropriate Luggin capillary.

Electrodepositions were carried out in a one-compartment cell made of Pyrex glass and with a Teflon cover having adequate holes to lodge the electrodes, entrances to add reagents to the bath and the thermometer. The solution inside the cell had an initial volume of 50 ml and was agitated by means of a magnetically driven stirrer that also served as a heat source. The electrolytic bath was of the conventional Watts type modified by the addition of $CoSO_4$ and/or $ZnCl_2$ in the required amounts. All solutions were prepared with Merck PA reagents dissolved in water purified by a Milli-Q system from Millipore.

The plating of the mild steel substrates was performed in a galvanostatic mode with a potentiostat/galvanostat (model 371 EGG&PARC). The $ZnSO_4$ stock solution was added to the bath using a mod. 682 metrohm titroprocessor provided with a Dosimat microburet. The electrodeposits were analysed with an energy dispersive X-ray (EDX) microanalyser (Link Analytical model (QX 2000) and with a scanning electron microscope (Zeiss DSM 960). Chemically dissolved deposits were analysed by atomic absorption using a spectrometer (Hitachi model Z810) and by differential pulse polarography using a polarographic analyser (model 348B EGG&PARC) and an electrode system (model 303A EGG & PARC). For the other electrochemical measurements a potentiostat (model 273 EGG&PARC) and a recorder (model 7046B Hewlett-Packard X–Y) were used.

3. Results and discussion

3.1. *Ni and Ni–Co alloys electrodeposition*

Figure 1 shows a flowchart of the deposition methodology specially developed to produce deposits showing the following characteristics: (a) a multilayer structure; (b) an enhanced adherence resulting from the absence of Zn in contact with the substrate and; (c) a Zn concentration profile increasing from the inner part to the surface of electrodeposits. In the first step, the objective was to deposit a nickel layer on the substrate to improve the adherence and to minimize the possibility of exposure of the mild steel base during utilization. After this step, the addition of the cobalt salt to the bath resulted in a smooth Ni–Co layer with a composition similar to the external region, that provided an enhanced physical stability of the porous structure. In this case, four different compositions were prepared. In the case of pure nickel deposits this step was not included in the sequence. The next step was the slow addition of Zn^{2+} to the eletrolyte. As a consequence, the zinc content in the alloy grew as the deposition was carried out. In the last step, the bath composition was kept constant with respect to $[Zn^{2+}]$ to allow the growth of a layer of high porosity in the electrodeposit. The subsequent activation of the deposits by means of alkaline leaching is much more efficient here than in Ni–Zn or Ni–Co–Zn alloys obtained in the traditional manner [9] thus producing a highly porous surface and the almost total elimination of zinc from the deposited layer (see below).

3.2. *SEM and EDX analysis of the electrodeposits structure*

The multilayer nature of the alloys prepared using the

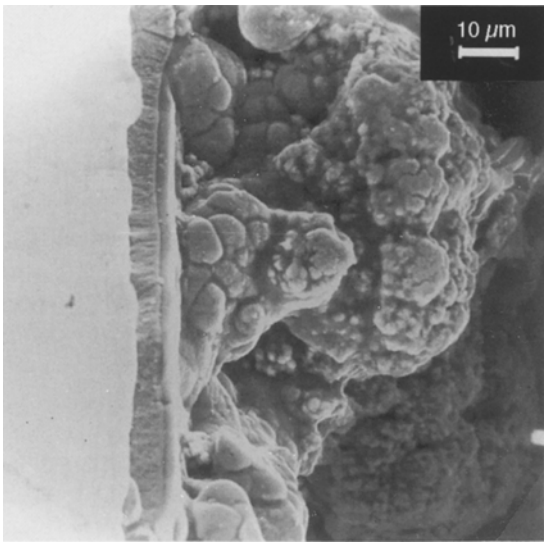

Fig. 2. SEM picture for a transverse section of a Ni–Co–Zn deposit (47 at % Co) showing the multilayer character of the deposit. The first bright layer on the left hand side is the mild-steel substrate, the second layer is pure nickel, the third very thin layer corresponds to Ni–Co and the last one (very porous) is of Ni–Co–Zn.

methodology above is exemplified in Fig. 2 by a SEM picture of a transverse section of a deposit obtained from a bath containing 100 g dm^{-3} $CoSO_4$. On the left hand side of the deposit a bright region reveals the mild steel substrate. Following this there is a smooth layer of pure nickel, a very thin and smooth layer of Ni–Co and finally the rough layer of Ni–Co–Zn. This picture illustrates the objective of the developed methodology for the deposition of new types of Ni–Zn and Ni–Co–Zn alloys.

As shown before, the multilayer deposition of Ni, Co and Zn produces an alloy with a very specific distribution of the atoms of each metal. To determine such a distribution, an EDX analysis of a transverse section of a nonactivated deposit obtained from a bath containing 100 g dm^{-3} $CoSO_4$ was carried out. Figure 3 shows the corresponding concentration lines in arbitrary units; these were adjusted in each measurement to avoid overloading the scale. The lines are plotted against a background of Fig. 2 for better understanding. The multilayer nature of the deposits is clear. Thus, a Ni region of about 15 μm is observed immediately above the mild steel substrate (Ni curve). The next region of the deposit (~5 μm) shows an increase in the Co EDX line (Co curve) caused by the addition of Co^{2+} to the plating bath, with the consequent decrease of the Ni line, revealing the formation of the Ni–Co layer. In the last region, the Zn line (Zn curve) increases while those for Co and Ni diminish. This last layer has a thickness greater than 15 μm and, after leaching, produces a very porous surface.

3.3. *Chemical analysis of the alloys*

The chemical analysis of the total amount of zinc in the electrodeposits after alkaline leaching, as well as the determination of the Ni–Co layer composition, was done using two different techniques, that is, differential pulses polarography (DPP) and atomic absorption spectrophotometry (AAS). For that purpose, Ni–Co deposits containing different amounts of Co were prepared following the flowchart procedure (Fig. 1) but without applying the first step corresponding to the pure nickel layer. These deposits were initially dissolved in 'aqua regia' avoiding excessive dissolution of the mild steel substrate, followed by prolonged heating to remove nitrate by thermal decomposition. The resulting solutions were conveniently diluted for the analyses. In the case of AAS, the dilution was made directly with water while for the polarographic analyses the following electrolytes were used: (a) 1 M NH_4Cl/NH_3 for Ni and Zn determinations and (b) 1 M $NH_4Cl/NH_3 + 0.2$ M $NO_2^- + 10^{-3}$ M dimethylglyoxime for Co [17]. The results of these analyses for the four Ni–Co alloys

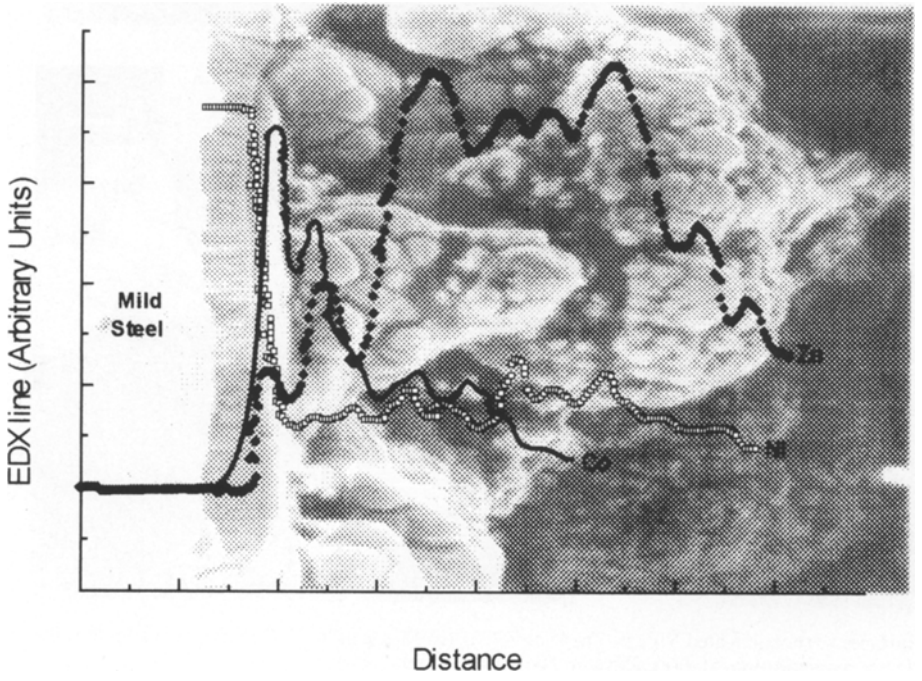

Fig. 3. Energy Dispersive X-ray analysis (EDX) of Ni, Co and Zn on a transverse section of a nonactivated Ni–Co–Zn electrodeposit (47 at % Co) plotted against a background of Fig. 2.

Table 1. Ni, Co and Zn compositions in the different deposits measured by atomic absorption spectrophometry (AAS) and differential pulse polarography (DPP)

$[CoSO_4]$ (*in the bath*) $g\,dm^{-3}$	*Ni/at %*		*Co/at %*		*Zn/at %*
	AAS	*DPP*	*AAS*	*DPP*	*AAS/DPP*
50	69	73	31	27	nd
100	58	53	42	47	nd
150	35	41	65	59	nd
200	26	30	74	70	nd

nd = not detected.

investigated are presented in Table 1. They demonstrate that the proposed methodology for electrodeposition yields alloys that permit the total removal of Zn within the detection limits of the analytical techniques employed here. Similar results were obtained for the samples containing only Ni. Table 1 also show that the Co composition in the deposit is always proportional to the Co^{2+} concentration in the plating bath.

3.4. *Topological analysis of the surfaces*

Figure 4 collects the SEM results obtained for the surface of a deposit with 47 at % of Co. Figure 4(a) shows the picture obtained for the non-activated surface while Fig. 4(b) and (c) correspond to the same surface after alkaline leaching, for different magnifications. Finally, and for comparison, Fig. 4(d) shows a pure porous nickel surface obtained by deposition in the absence of cobalt and subsequent activation. The removal of zinc is clearly visible when comparing the two upper pictures through the disappearance of the dendritic structures usually associated with electrodeposited zinc. The remaining surface (Fig. 4(b)) shows a less porous columnar structure with numerous microcracks on the top. The extremely large area of these deposits (see later) is probably associated with those microcracks. Figure 4(c) shows details of these structures using an increased magnification (5000×) while Fig. 4(d) shows the nickel surface with the same magnification. Here, the presence of microcracks cannot be

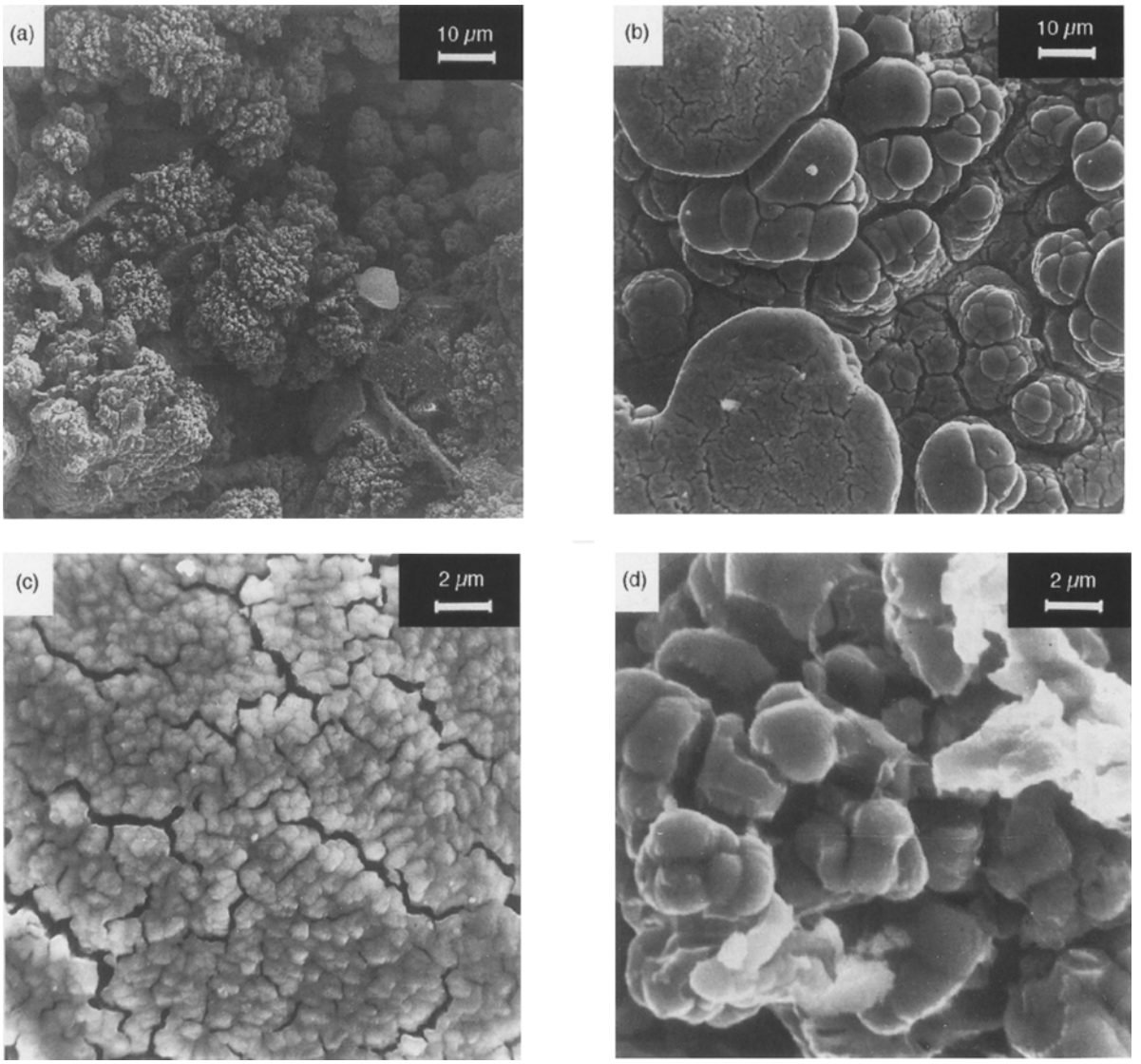

Fig. 4. SEM pictures of the following surfaces: (a) nonactivated Ni–Co–Zn (47 at % Co), (b) Ni–Co (47 at % Co) after activation by alkaline leaching, (c) same as (b) but for a different magnification, and (d) activated Ni.

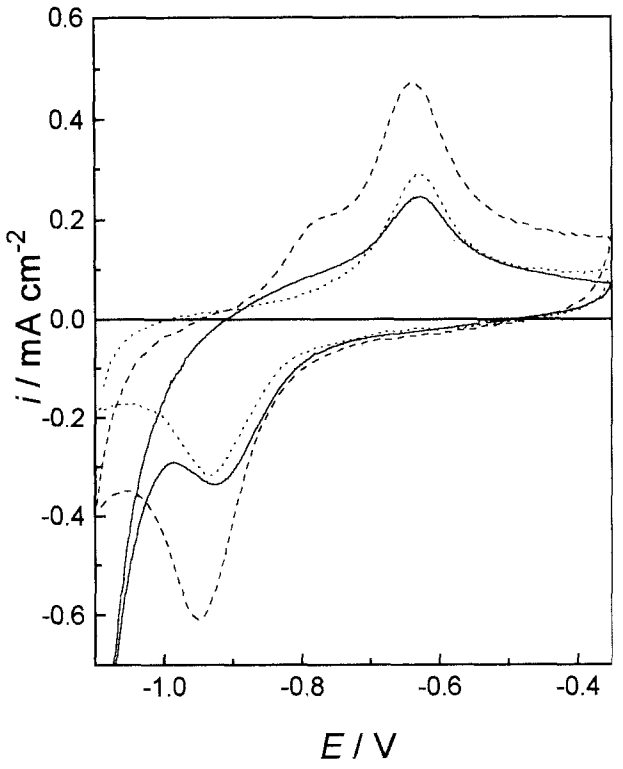

Fig. 5. Cyclic voltammograms for bright nickel in the steady state (full line) and for a 1:1 Ni–Co metallurgical alloy in the first (dashed line) and after 20 cycles (dotted line) in 0.5 M NaOH at 50 mV s^{-1} in the potential region of formation and reduction of α-$Ni(OH)_2$.

observed but again the picture reveals a very large surface area.

3.5. *Voltammetric evaluation of the electrochemical active area*

The method used here to evaluate the electrochemical active area of Ni and Ni–Co surfaces is based on the cyclic voltammetric oxidation of the nickel surface to form one complete monolayer of α-$Ni(OH)_2$ [9, 18]. In this case, the peak currents are directly proportional to the exposed nickel area. In addition, it has been shown previously [9] that the same methodology can be applied to Ni–Co surfaces. This is because the formation of $Co(OH)_2$ is irreversible in the potential range used [19] and its contribution to the anodic currents can be eliminated by cycling the electrode potential several times before collecting the data. This behaviour is shown in Fig. 5 which compares the cyclic voltammetric response in alkaline solutions of a bright nickel electrode (full line) with a 1:1 Ni–Co metallurgical alloy in the first cycle (dashed line) and after stabilization (dotted line). The voltammograms were recorded in 0.5 M NaOH at room temperature and at 50 mV s^{-1}. From Fig. 5 it is clear that on the first cycle the anodic peak of the Ni–Co surface comprises two different processes, that is, the formation of $Co(OH)_2$ and α-$Ni(OH)_2$, respectively. However, after 20 cycles the Ni–Co response becomes very similar to that of the pure nickel electrode, except perhaps by the less marked activity for hydrogen evolution (cathodic extreme of the voltammogram). The small differences in peak current densities may be attributed to variations in the roughness factors of the electrodes due to different hardness of the materials. Meanwhile, the voltammetric response in that restricted potential range can still be used as a good approximation for the measurement of the electrochemical active area of porous Ni–Co alloys, in a similar manner to that described for porous nickel electrodes [9, 16].

Thus, Fig. 6 presents the steady-state cyclic voltammograms obtained for the porous electrodes under the same experimental conditions. The full

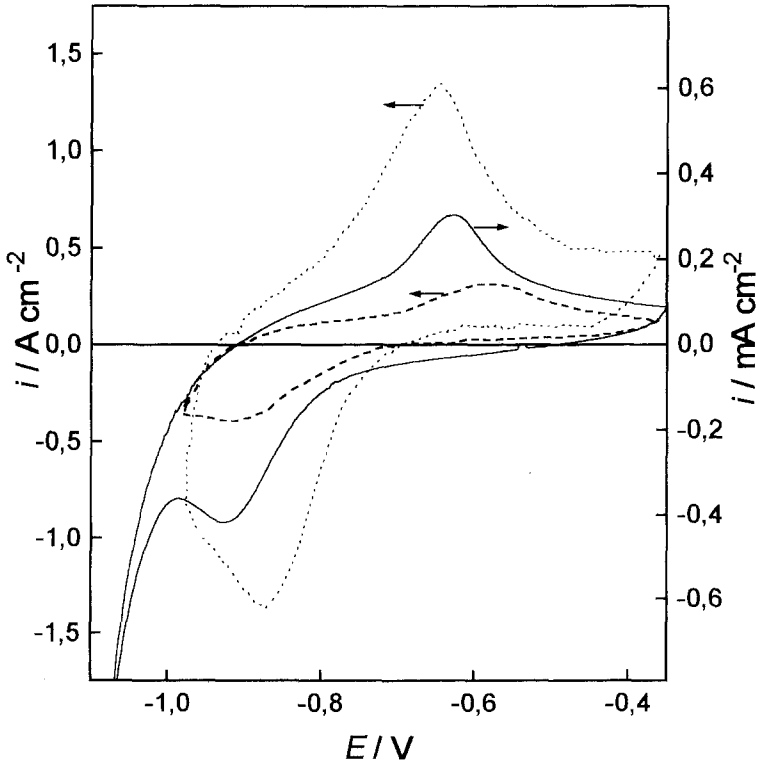

Fig. 6. Cyclic voltammograms for bright nickel (full line), porous nickel (dashed line), and porous Ni–Co (dotted line) in 0.5 M NaOH at 50 mV s^{-1} in the potential region of formation and reduction of α-$Ni(OH)_2$.

Table 2. Tafel parameters for the HER on high area Ni and Ni–Co electrodes at several temperatures

T/°C	*Ni*		*Ni–Co*	
	Tafel slope /mV dec.$^{-1}$	$i_0 \times 10^4$ /A cm^{-2}	*Tafel slope* /mV dec.$^{-1}$	$i_0 \times 10^3$ /A cm^{-2}
25	85	5.75	70	1.74
35	87	9.02	66	2.11
45	76	9.88	66	2.56
55	77	14.70	61	3.29
65	78	26.50	53	3.76
75	81	41.70	–	–

line corresponds to bright nickel and is included for comparison while the dashed line and the dotted line are for large area (porous) Ni and Ni–Co (47 at % Co) electrodes, respectively. From equivalent voltammograms, but using electrodes with different Co concentration in the alloy, it was observed that: (i) the mean roughness factor was about 4400 for the porous Ni–Co alloys and 1100 for the porous Ni, and (ii) the former value is practically independent of the Co concentration in the deposit.

3.6. *Long-term water electrolysis*

To verify the activity toward the HER of the large area deposits obtained by the procedure described above, steady-state polarization experiments at several temperatures and long-term water electrolysis tests were performed. The electrochemical parameters extracted from the Tafel plots are present in Table 2. Although the current density values are relatively low, the activity towards the HER at high current densities is a consequence of the values of the Tafel slopes. As can be observed from Table 2, these values are considerably lower than those expected for a one electron reaction (i.e., 2.303 $RT/0.5F$). Such behaviour is in perfect agreement with results previously published for porous surfaces [1, 3, 9]. More detailed information on this kind of studies can be found elsewhere [9]. For the long-term electrolysis the conditions were analogous to those used in industrial unipolar water electrolysers, that is, applying 135 mA cm^{-2} at 70 °C and using 6 M KOH as the electrolyte. The measured potentials are presented in Fig. 7 as a function of time. Three kinds of cathodes with the same geometric area were used. The different curves refer to (a) smooth mild-steel cathode, (b) large area Ni, (c) large area Ni–Co (47 at % Co in the deposit), and (d) the same Ni–Co electrode but at 250 mA cm^{-2}. Potential values taken after stabilization at around 100 h, show that the porous alloys operate at potentials approximately 300 mV less cathodic than the mild steel electrode and with overpotentials lower than 100 mV. This is clear evidence of the enhanced activity of the alloys toward the HER. In this same way, the activity of large area Ni–Co is slightly greater than that of nickel electrodes. In both cases, the stability of the active coatings for long term operation under laboratory conditions was well established.

4. Conclusions

The new methodology presented in this work proved to be effective for the preparation of large area Ni and Ni–Co coatings having a multilayer structure. The distribution of the inner layers in the deposits confirms the objectives of the deposition methodology and points to a superior physical resistance of these active materials when compared to the traditional ones. The morphology of the coatings shows that the large surface area is associated with a columnar type structure which, in the case of Ni–Co, also presents numerous microcracks on the surface. The voltammetric results used for real electrochemical

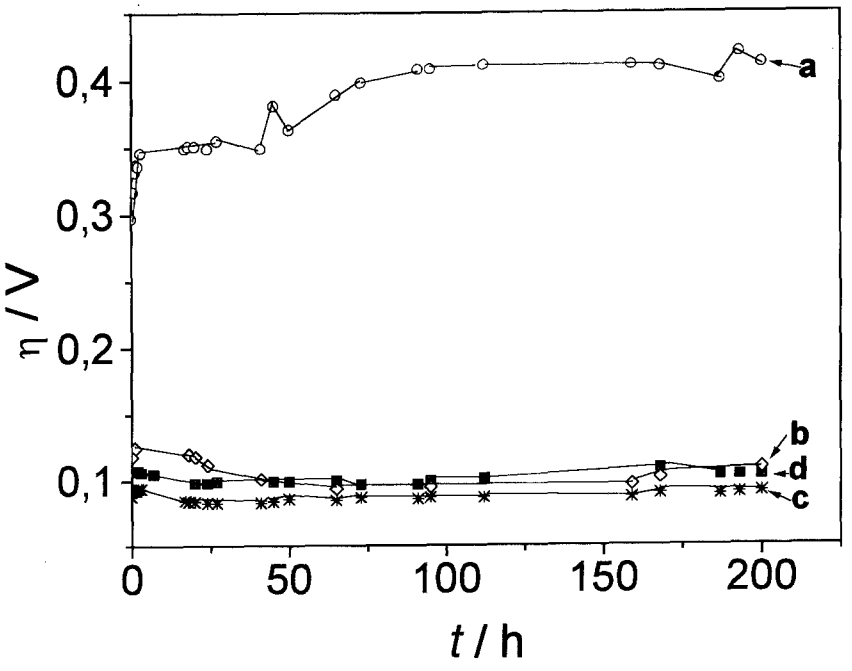

Fig. 7. Long-term operation water electrolysis in 6 M KOH at 70 °C. The lines correspond to (a) smooth mild-steel, (b) porous Ni and; (c) porous Ni–Co at 135 mA cm^{-2} while curve (d) is for porous Ni–Co at 250 mA cm^{-2}.

area evaluation confirm these conclusions showing also that, in the case of nickel, where the microcracks are not present, the roughness factor is lower than for Ni–Co.

Analysing the behaviour of these electrodes for the hydrogen evolution reaction, it can be concluded that the real electrochemical area plays a very important role in the electrochemical activity. Such electrodeposits are, in a broad sense, very convenient materials for use as cathodes in water electrolysis or as precursors for other large area structures.

Acknowledgements

The authors wish to thank FINEP, CNPq and CAPES for the financial support of this work. They also thank Eng. Marcelo A.P. da Silva from IFSC–USP for the SEM and EDX analyses.

References

[1] B. V. Tilak, A. C. Ramamurthy and B. E. Conway, *Proc. Indian Acad. Sci. (Chem. Sci.)* **97** (1986) 359.
[2] Y. Choquette, H. Ménard and L. Brossard, *Int. Hydrogen Energy* **14** (1989) 637.
[3] M. J. de Giz, S. A. S. Machado, L. A. Avaca and E. R. Gonzalez, *J. Appl. Electrochem.* **22** (1992) 973.
[4] Th. Borucinski, S. Rausch and H. Wendt, *ibid.* **22** (1992) 1031.
[5] J. de Carvalho, G. Tremiliosi-Filho, L. A. Avaca and E. R. Gonzalez, *Int. J. Hydrogen Energy* **9** (1989) 165.
[6] M. J. de Giz, M. Ferrereira, G. Tremiliosi-Filho and E. R. Gonzalez, *J. Appl. Electrochem.* **23** (1993) 641.
[7] M. Spasojevic, N. Krstajic, P. Despotov, R. Atanasoski and K. Popov, *ibid.* **14** (1984) 265.
[8] I. Arul Raj and K. I. Vasu, *ibid.* **20** (1990) 32.
[9] S. A. S. Machado, P. de Lima Neto, J. Tiengo and L. A. Avaca, *Electrochim. Acta* **39** (1994) 1757.
[10] J. E. Bennett and H. G. Tompkins, *J. Electrochem. Soc.* **123** (1976) 999.
[11] L. Chen and A. Lasia, *ibid.* **136** (1991) 3321.
[12] J. Balej, J. Divisek, H. Schmitz and J. Mergel, *J. Appl. Electrochem.* **22** (1992) 711.
[13] A. Brenner, 'Electrodeposition of Alloys', vol. 2, Academic Press, New York (1963) pp. 194–238.
[14] W. E. Triaca, A. J. Arvia and T. Kessler, *J. App. Electrochem.* **23** (1993) 655.
[15] H. Alemu and K. Juttner, *Electrochim. Acta* **33** (1988) 1101.
[16] H. Wendt and V. Plizak, *ibid.* **28** (1983) 27.
[17] A. Bobrowski, *Anal. Chem.* **61** (1989) 2178.
[18] S. A. S. Machado and L. A. Avaca, *Electrochim. Acta* **39** (1994) 1385.
[19] H. G. Gomez Meier, J. R. Vilche and A. J. Arvia, *J. Electroanal. Chem.* **134** (1982) 251.